# The Response of the Stratospheric Climate to Projected Changes in the Concentrations of Well-Mixed Greenhouse Gases from 1992 to 2051

Neal Butchart, John Austin, Jeffrey R. Knight, Adam A. Scaife, and Mark L. Gallani

*The Met. Office, Bracknell, Berkshire, United Kingdom*

## ABSTRACT

Results are presented from two 60-yr integrations of the troposphere–stratosphere configuration of the U.K. Met. Office's Unified Model. The integrations were set up identically, apart from different initial conditions, which, nonetheless, were both representative of the early 1990s. Radiative heating rates were calculated using the IS92A projected concentrations of the well-mixed greenhouse gases (GHGs) given by the Intergovernmental Panel on Climate Change, but changes in stratospheric ozone and water vapor were not included. Sea surface conditions were taken from a separate coupled ocean–atmosphere experiment. Both integrations reproduced the familiar pattern of tropospheric warming and a stratospheric cooling increasing with height to about $-1.4$ K per decade at 1 mb. There was good agreement in the trends apart from in the polar upper stratosphere and, to a greater extent, the polar lower-to-middle stratosphere, where there is significant interannual variability during the winter months. Even after decadal smoothing, the trends in the northern winter were still overshadowed by the variability resulting from the planetary wave forcing from the troposphere. In general, the decadal variability of the Northern Hemisphere stratosphere was not a manifestation of a uniform change throughout each winter but, as with other models, there was a change in the frequency of occurrence of sudden stratospheric warmings. Unlike previous studies, the different results from the two simulations confirm the change in frequency of warmings was due to internal atmospheric variability and not the prescribed changes in GHG concentrations or sea surface conditions. In the southern winter stratosphere the flux of wave activity from the troposphere increased, but any additional dynamical heating was more than offset by the extra radiative cooling from the growing total GHG concentration. Consequently the polar vortex became more stable, with the spring breakdown delayed by 1–2 weeks by the 2050s. Polar stratospheric cloud (PSC) amounts inferred from the predicted temperatures increased in both hemispheres, especially in the early winter. In the Southern Hemisphere, the region of PSC formation expanded both upward and equatorward in response to the temperature trend.

## 1. Introduction

In contrast to the enormous international effort made to predict the response of surface meteorological parameters to projected changes in greenhouse gas (GHG) concentrations [e.g., see Table 6.3 of Houghton et al. (1996)], climate change in the stratosphere has, until recently, received very little attention. Indeed, most of the general circulation models (GCMs) used for climate prediction have very poor vertical resolution in the stratosphere, though in some the vertical domain has been extended to allow for a more comprehensive treatment of the middle atmosphere (e.g., see Hamilton 1996). However, only a few of these extended models (e.g., Mahfouf et al. 1994; Rind et al. 1998) have been used in estimating the future state of the stratosphere. Therefore, additional simulations are required to determine with confidence the likely atmospheric changes. In this paper we present new predictions obtained from the troposphere–stratosphere configuration of the U.K. Meteorological Office (UKMO) "Unified Model" (UM; Cullen 1993; Butchart and Austin 1998).

Changes in stratospheric climate are particularly important because of the consequences for ozone depletion (e.g., see World Meteorological Organization 1999, chapter 12). For example, Austin et al. (1992; see also Austin and Butchart 1994) showed that, with chlorine abundances of the late 1980s, doubling $CO_2$ could enhance the prospect of an Arctic ozone hole, though the actual phasing out of chloroflurocarbons is expected to lead to an eventual reduction in the losses of polar stratospheric ozone. Nonetheless, Shindell et al. (1998) have shown that, despite chlorine decreases, ozone losses over the Arctic could still increase, and the eventual recovery be delayed, if the climate change associated with increasing GHG concentrations is taken into account. Therefore, to investigate this further we have integrated the troposphere–stratosphere configuration of the UM for a 60-yr period starting from conditions of

the early 1990s. Radiative heating rates within the model were calculated using projected concentrations of the well-mixed GHGs (see section 3). Sea surface temperatures (SSTs) and sea ice extents prescribed at our model lower boundary were computed (Mitchell et al. 1995) using a coupled ocean–atmosphere version of the UM that did not have the extended vertical domain (again see section 3).

Both Austin et al. (1992) and Shindell et al. (1998) found that the response of polar ozone in their models was determined to a large extent by the changes in circulation. In particular the models tended to produce a colder more stable polar vortex when GHG concentrations were increased, consistent with recent observed trends (Zurek et al. 1996; Pawson and Naujokat 1997). Shindell et al. attribute this to a reduction in the frequency of occurrences of sudden stratospheric warmings in their experiment but could not establish to what extent this conclusion was model dependent. Despite this uncertainty their results clearly demonstrated that predicting future ozone depletion will depend critically on the response to climate change of the planetary wave forcing of the stratospheric circulation during winter and spring. Therefore in our analysis of the UM's predictions we focus on these aspects of the modeled response as well as the more basic trends in the global and annual mean temperatures. We also examine the effect of modeled temperature changes on the formation of polar stratospheric clouds (PSCs).

## 2. Model description

The troposphere–stratosphere configuration of the UM used for this study was an improved version of the middle atmosphere GCM described in Butchart and Austin (1998). The latitude–longitude resolution was $2.5° \times 3.75°$ and there were 49 vertical levels extending from the surface to 0.1 mb, with levels roughly every 1.3 km throughout the stratosphere. The physical parameterizations were upgraded from those based on the "HadAM2b" build[1] of the 19-level (upper boundary 4.6 mb) climate configuration of the UM, used by the UKMO's Hadley Centre, to those based on the "HadAM3" build. Details of the upgrades are given in Pope et al. (2000). In particular we employed the Edwards and Slingo (1996) radiative transfer algorithm, which allowed contributions to the longwave cooling from the well-mixed GHGs—$CH_4$, $N_2O$, CFC11, and CFC12, as well as $CO_2$. We also changed the orographic gravity wave–drag scheme from that based on Palmer et al. (1986) to the more sophisticated scheme described in Gregory et al. (1998), which is currently considered

the best choice for most UM applications. As in Butchart and Austin (1998), the gravity wave–drag scheme was replaced by Rayleigh friction above 20 mb with the coefficient given by the dashed curve in their Fig. 1. This combination of parameterized gravity wave–drag and Rayleigh friction is the same as that used by Swinbank et al. (1998).

Some other changes from Butchart and Austin (1998) are worth noting. First, there was the switch from a 15- to a 30-min time step for the physical processes. This is the same time step as used in the HadAM3 build of the climate configuration and is therefore more consistent with any "tuning" of the parameterizations to suit the choice of time step. To ensure numerical stability in the stratosphere and mesosphere, however, we continued to use a 15-min time step for the dynamics (i.e., two "sweeps" of the dynamics routines were performed for each time step of the physical parameterizations). Second, the numerical stability of the model at upper levels was improved by revising the reference temperature profile used in the time integration (Cullen and Davies 1991). Finally, the horizontal diffusion was slightly increased in the model's top two levels. First-order diffusion was now used on both these levels with the coefficient increased from $4.0 \times 10^6$ s$^{-1}$ to $4.8 \times 10^6$ s$^{-1}$ at the top level and a coefficient of $6.7 \times 10^5$ s$^{-1}$ used at the level below that.

These changes improved the model's climatology compared to that reported in Butchart and Austin (1998). The subtropical and polar night jets were better separated in the Southern Hemisphere when the new gravity wave–drag scheme was used, as in Swinbank et al. (1998). Changing to the Edwards and Slingo (1996) radiation scheme reduced the model's overall cold bias throughout the stratosphere so that the simulated temperatures with the current version of the model were on average about 10–15 K higher at the stratopause level compared to the results of Butchart and Austin (1998) and Swinbank et al. (1998). The model's previous substantial overprediction of the stationary wave amplitudes in the Southern Hemisphere (Butchart and Austin 1998; Swinbank et al. 1998) was also significantly improved (D. Jackson 1999, personal communication). In addition, interannual variance in the winter stratosphere was found to be more realistic, especially in the Southern Hemisphere where the model now reproduced the observed double maximum in the standard deviation of the July mean westerly jet (D. Jackson 1999, personal communication; Butchart and Austin 1998, Fig. 10). Despite these improvements, the model still had deficiencies such as a "cold pole" and the incorrect tilt with height of the polar-night jet, but these problems afflict most middle atmosphere GCMs (Pawson et al. 2000; World Meteorological Organization 1999, section 7.5.2).

## 3. Experimental design

The model was initialized with assimilated observations (Swinbank and O'Neill 1994) for 28 February

---

[1] Butchart and Austin (1998) referred to this as "3CV" but the Hadley Centre subsequently standardized their naming convention for builds of the Atmosphere Model to the form "HadAMn," where n denotes the build number.
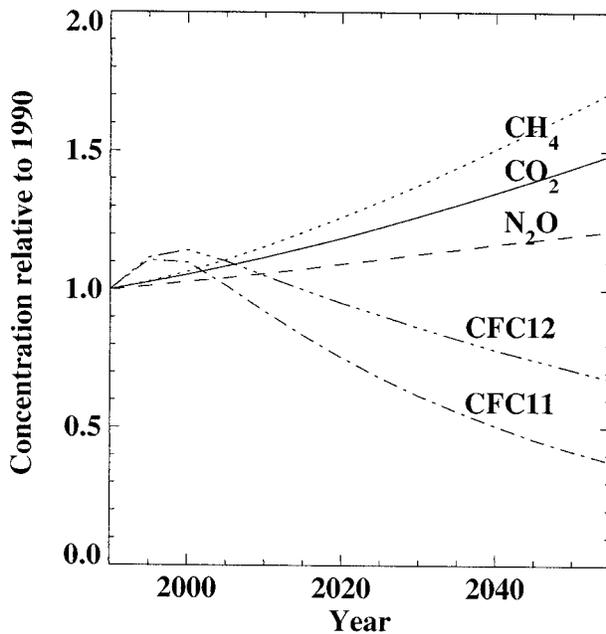
FIG. 1. GHG concentrations used in the climate change simulations relative to 1990 values of 351 ppmv, 1.7 ppmv, 310 ppbv, 263 pptv, and 477 pptv, for $CO_2$, $CH_4$, $N_2O$, CFC11, and CFC12, respectively.

1989 and integrated for almost 63 yr until 31 December 2051. Concentrations of the well-mixed GHGs were taken from the Intergovernmental Panel on Climate Change (IPCC) scenario IS92a (Houghton et al. 1996, chapter 2) with $CO_2$, $CH_4$, and $N_2O$ increasing steadily throughout the integration but with CFC11 and CFC12 decreasing after 1995 and 2000, respectively (see Fig. 1). The scenario assumed for these gases, particularly $CH_4$, CFC11, and CFC12 has now undergone further revision and current recommendations are somewhat lower for $CH_4$ (World Meteorological Organization 1999, chapter 11), although the absence of these revisions from our study is thought unlikely to affect the conclusions since it represents only a small adjustment to the radiative forcing. More importantly, the distributions of all the well-mixed GHGs were assumed spatially and seasonally independent, which is, perhaps, less appropriate for the stratosphere. Also, we used a zonally symmetric seasonally varying ozone climatology based on Keating et al. (1987) above 22 mb, and reprocessed solar backscatter ultraviolet (UV) data for 1979–81 below 22 mb. Therefore, no account was taken in this particular experiment of any possible future changes in stratospheric ozone amounts.

The transient response of the climate to increasing GHG concentrations is known to depend on the complex feedback between the oceans and the atmosphere (Houghton et al. 1996, chapter 6). However, we avoided the computational expense of a fully coupled ocean–atmosphere GCM (OAGCM) by prescribing at our model lower boundary SSTs and sea ice extents from an independent OAGCM experiment. These were updated

every 5 days by interpolating between monthly mean values obtained from an experiment carried out using a version of the UM in which the atmosphere component was HadAM2b (Mitchell et al. 1995; Johns et al. 1997; Mitchell and Johns 1997). Support for this approach is given by Timbal et al. (1997), who showed that, even when the SST anomalies from a coupled experiment are used to force a different atmospheric GCM, the general features of the atmospheric response driven by oceanic warming are reproduced. Apart from the ocean component, differences between the version of the UM we used and that used in the coupled experiment lie only in the upgrade of some of the physical parameterizations (see section 2) and, of course, the extended vertical domain with improved vertical resolution in the stratosphere.

A 20-yr reference integration was performed with GHG concentrations fixed at the corresponding 1995 values from the transient climate simulation. The SSTs and sea ice extents were from a 20-yr period starting at 1990 of the control integration of the coupled OAGCM [see Johns et al. (1997) for details]. This reference integration provided a check on the stability of the simulated climate and enabled us to separate actual trends from "model drift." It also allowed us to identify (see section 2) how the climatology of the current version of the model differed from that documented in Butchart and Austin (1998), although it was not possible to make a direct comparison because of the slightly different concentration of $CO_2$ used, and the different lower boundary conditions.

Last, during the course of the transient simulation (run "A") an error was discovered in the experiment setup that caused the model to use incorrect ozone solar heating rates in January 1990 and 1991. The integration was repeated (run "B") starting again from 28 February 1989, but because of the relatively short radiative timescale of the stratosphere, it is unlikely that the error had any effect in the original simulation after January 1992, apart from those aspects resulting from the chaotic behavior of the system. We therefore made use of both simulations and analyzed the 60-yr period 1992–2051 in the two integrations to separate chaotic variability from the underlying trends.

## 4. Temperature trends 1992–2051

### a. Annual mean

The predicted global change in the annual mean temperatures was almost identical for the two simulations (cf. Figs. 2a and 2b). As expected, the increasing GHG concentrations produced a cooling of the stratosphere and a warming of the troposphere. Also, as might be expected, the surface responses in both simulations (not shown) were similar to the coupled OAGCM experiment (Mitchell and Johns 1997) that provided our SST and sea ice boundary conditions. Both runs produced the
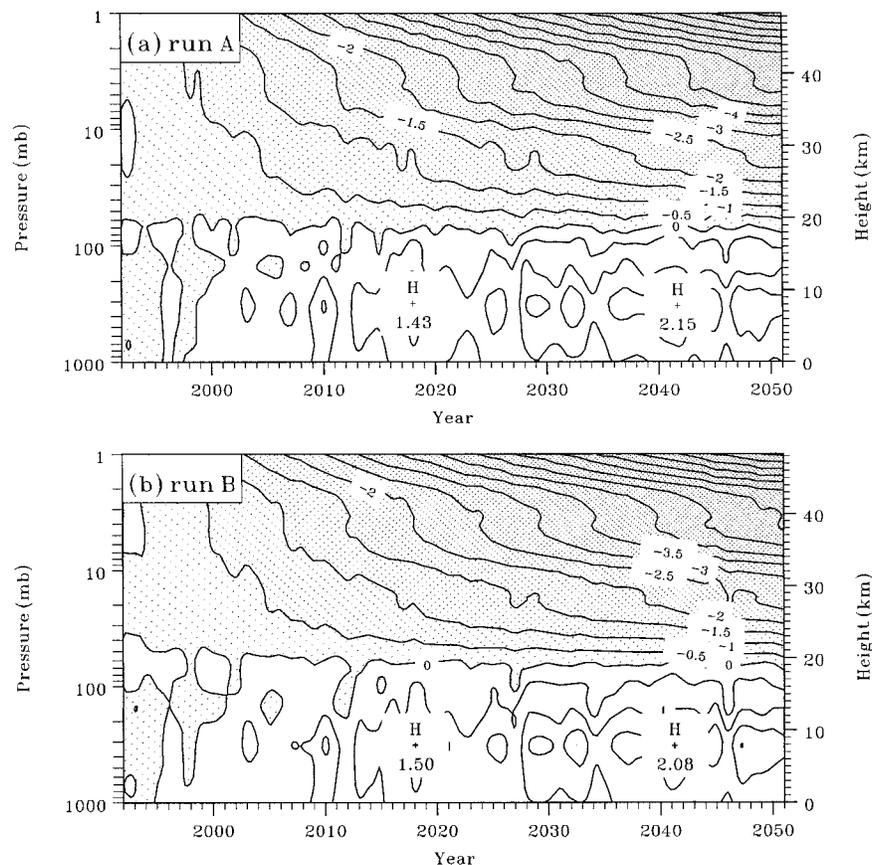
FIG. 2. Change, from 1992, in the globally and annually averaged temperatures for (a) run A and (b) run B. Shading denotes a cooling, and the contour interval is 0.5 K.

same decadal variability in the tropospheric response, most likely because it was generated by an exchange of heat between the atmosphere and ocean, determined by the identical SST and sea ice extents. These effects did not significantly extend above the tropopause, at least for the global and annual mean, and the steady cooling of the stratosphere seen in Figs. 2a and 2b indicates the more direct radiative influence of the increasing GHG concentrations there. This is further highlighted by both runs producing almost identical increases in cooling with height. This is a purely radiative feature resulting from increased concentrations of GHGs enhancing both the emission and absorption of thermal infrared (IR) radiation. In the lower stratosphere the cooling due to enhanced IR emission is offset by the effects of increased absorption of upwelling IR radiation from the troposphere, hence the greater cooling with height throughout the stratosphere. The balance between increased absorption and emission is, however, not the same for the individual GHGs at each level in the stratosphere (e.g., World Meteorological Organization 1999, section 5.3.2), and this may be the reason why there was a layer near 40 km in both runs where the cooling rate was constant with height (cf. Figs. 2a and 2b). Similar temperature diagnostics (not shown) for the ref-

erence simulation show that, without any prescribed changes in the GHG concentrations and sea surface boundary conditions, stratospheric temperatures remained almost constant, with no apparent trend in the tropospheric temperatures. The latter were, however, not constant, presumably because of the effects of the oceans, which again did not appear to extend above the tropopause, at least in the global and annual mean.

Figure 3a shows, for run A, the trends in the zonally averaged annual mean temperature for 1992–2051 as a function of latitude and height. Well established features of climate change, such as the enhanced surface warming toward the North Pole and the maximum warming in the equatorial upper troposphere (e.g., Mahfouf et al. 1994), were well reproduced. In the troposphere and lower stratosphere the pattern is similar to that reported by Mitchell and Johns (1997) for their coupled OAGCM experiment using a version of the UM without the extended vertical domain. For the upper stratosphere, the trends are broadly in agreement with those that can be inferred from doubled-$CO_2$ experiments with stratospheric models (Pitari et al. 1992; Mahfouf et al. 1994; Rind et al. 1998), but are slightly less than the past trends observed from space for the period 1979–97 [see Fig. 12 of Scaife et al. (2000)], when the concentrations
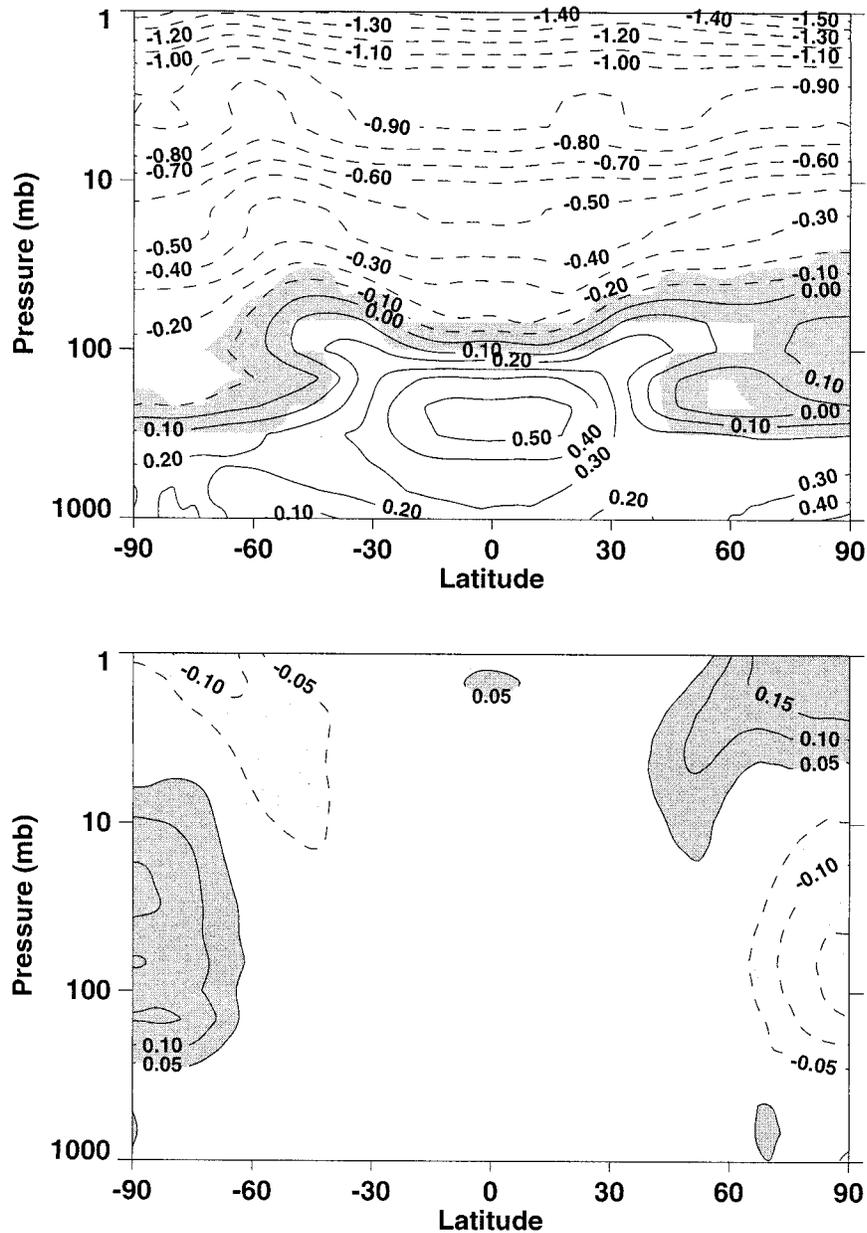
FIG. 3. (a: top) Best-fit linear trends for the zonally averaged annual mean temperatures for the period 1992–2051 for run A. Shading indicates where the trends are not significant at the 95% confidence level of a two-tailed $t$ test (assuming data for the individual years are independent). Dashed contours denote a cooling trend. The contour interval is 0.1 K decade$^{-1}$. (b: bottom) Trend in run B minus trend in run A. Dark (light) shading indicates where there is stronger (weaker) cooling, or weaker (stronger) warming in run A. The contour interval is 0.05 K decade$^{-1}$.

of $CO_2$, $CH_4$, and $N_2O$ increased at roughly the same rate as in our experiment. Over the same time ozone amounts decreased in the upper stratosphere and this alone was thought to have caused a cooling of about 0.3 K decade$^{-1}$ (e.g., World Meteorological Organization 1999, chapter 5). In contrast ozone amounts remained unchanged in our model integrations. In the lower stratosphere comparison with past trends is less useful because of the important contribution from ozone

changes (Ramaswamy et al. 1996), which were not considered in this study.

Despite producing similar patterns of trends, there were noticable differences between the two simulations over both polar regions, with an interesting compensatory structure between the upper and lower-to-middle stratosphere, and between each hemisphere (see Fig. 3b). Differences were relatively small (<10%) compared to the underlying trend in the upper stratosphere,
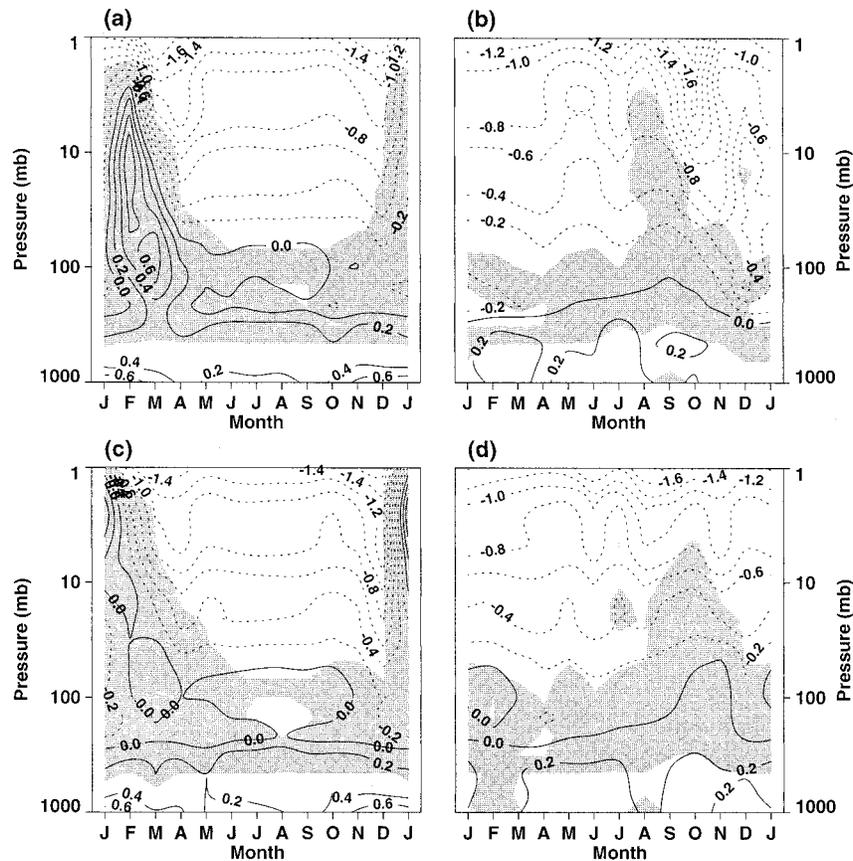
FIG. 4. Best-fit linear trends (K decade$^{-1}$) for the monthly mean temperatures averaged poleward of 60° for the period 1992–2051. (a) and (b) Northern and Southern Hemispheres, respectively, for run A. (c) and (d) Northern and Southern Hemispheres, respectively, for run B. Shading indicates that the trends are not significant at the 95% confidence level using the same $t$ test as in Fig. 3. Dashed contours denote a cooling trend. The contour interval is 0.2 K decade$^{-1}$.

but became much more significant in the lower stratosphere. In particular, run B did not produce the warming over the North Pole seen at about 100 mb in Fig. 3a, though this is perhaps not surprising given that the trend there was not statistically significant. Nonetheless, Mitchell and Johns (1997) found a similar north polar warming of the lower stratosphere, and it has been seen in other models (e.g., Mahfouf et al. 1994) in response to a doubling of $CO_2$. Mahfouf et al. attribute it to tropospheric changes due to increased $CO_2$ altering the dynamics of the stratosphere, but results from the two simulations presented here suggest that it may not be possible to predict reliably this effect from a single integration. There is a similar uncertainty in the response in the south polar lower stratosphere (see Fig. 3b). In contrast, Fig. 3b implies no lack of confidence in the response of the annual mean tropospheric temperatures in this experiment. The remaining regions where the trend is not significant are near the tropopause, which is the transition region between the tropospheric warming and stratospheric cooling responses to increased GHG concentrations. This transition region is at a slight-

ly higher altitude than would be expected from observations for 1979–95, probably due to the absence of ozone changes in the simulations (Hansen et al. 1998).

*b. Seasonal variations*

In both simulations the linear trend of the simulated monthly averaged zonal mean temperatures was fairly uniform throughout the year, apart from in the polar regions. There, the trend in the average temperatures poleward of 60° was significantly different during winter and spring (see Fig. 4). In the Southern Hemisphere, a statistically significant enhanced springtime cooling was predicted throughout most of the stratosphere by run A, and to a somewhat lesser extent by run B (cf. Figs. 4b and 4d). For the Northern Hemisphere both simulations again predicted statistically significant enhanced cooling of the upper stratosphere in spring, and also in early winter (Figs. 4a and 4c). On the other hand, a warming of the lower and middle stratosphere was predicted for February and March, but this was not statistically significant in either simulation. A comparison of the two
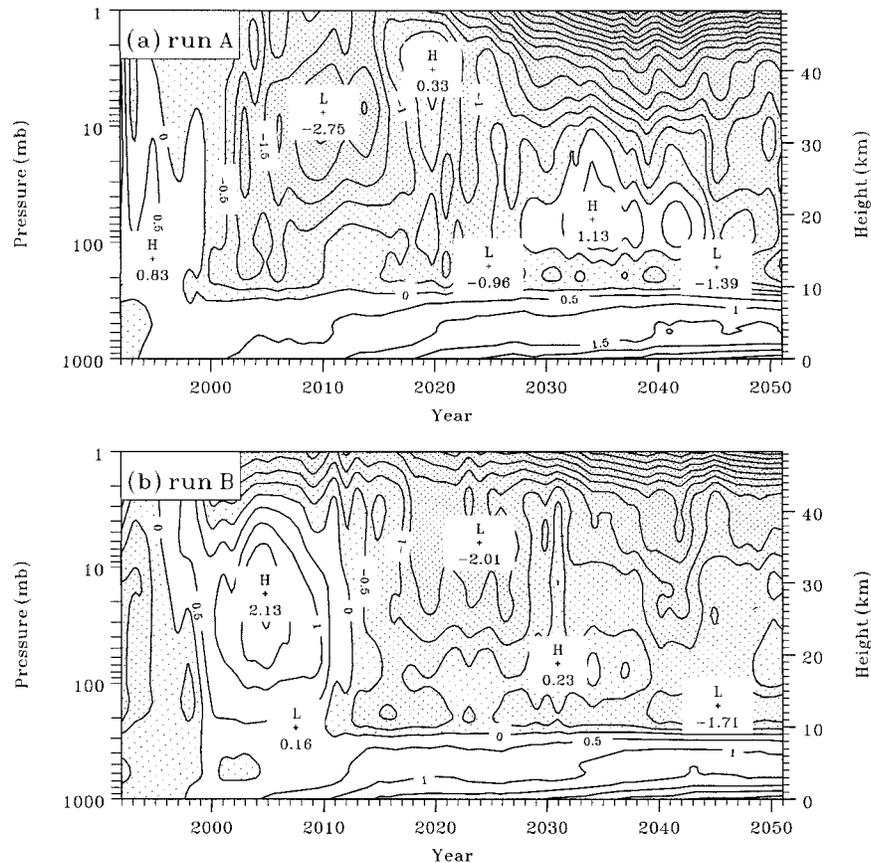
FIG. 5. DJF area-averaged temperature change poleward of 60°N for (a) run A and (b) run B. The changes are relative to the mean of the DJF area-averaged temperatures for 1992–2001 of the two simulations and have been smoothed by an 11-yr running mean. Shading denotes a cooling and the contour interval is 0.5 K.

simulations also indicates the unreliability of the quantitive predictions of the trends in polar temperatures during winter and spring. Nonetheless, the basic similarity between the two runs suggests that many of the features of the model's response may, at least, be qualitatively robust with the possibility, therefore, of serious ramifications for future ozone amounts (e.g., Shindell et al. 1998).

## 5. Northern Hemisphere winter

### a. Trends and low-frequency variability

One of the difficulties encountered in isolating trends in the polar stratosphere during the northern winter is the very large interannual variability resulting from the planetary wave forcing. Shindell et al. (1998) attempted to overcome this by considering decadal averages. Certainly the work of Scaife et al. (2000), based on almost 20 yr of observations, shows that an averaging period of the order of 10 yr should be sufficient to produce a statistically stable estimate of the climate of the stratosphere. Therefore, we have applied an 11-yr equally

weighted smoothing to the change in the mean December–February (DJF) averaged temperatures poleward of 60°N (see Fig. 5). For both simulations the changes are presented relative to the mean of the 10-yr DJF averages, 1991–2001, from the two simulations.

A notable feature of Fig. 5 is the distinct low-frequency variability of the lower-to-middle stratosphere and absence of any obvious trend from that region, in either simulation. This variability arose mainly from the dynamical forcing as indicated by the DJF mean Eliassen–Palm (EP) flux divergence (e.g., Andrews et al. 1987, section 3.5) poleward of 60°N, shown in Fig. 6 as the force per unit mass. Again the 11-yr smoothing has been applied to the data and the results are presented as a deviation from the 60-yr mean. Consistent with the transformed Eulerian mean formalism of wave-mean flow interaction [again see, e.g., Andrews et al. (1987, section 3.5)] there is good agreement between the periods of anomalous EP flux convergence (divergence) in the lower and middle stratosphere in Fig. 6 and the anomalously warm (cold) periods in Fig. 5.

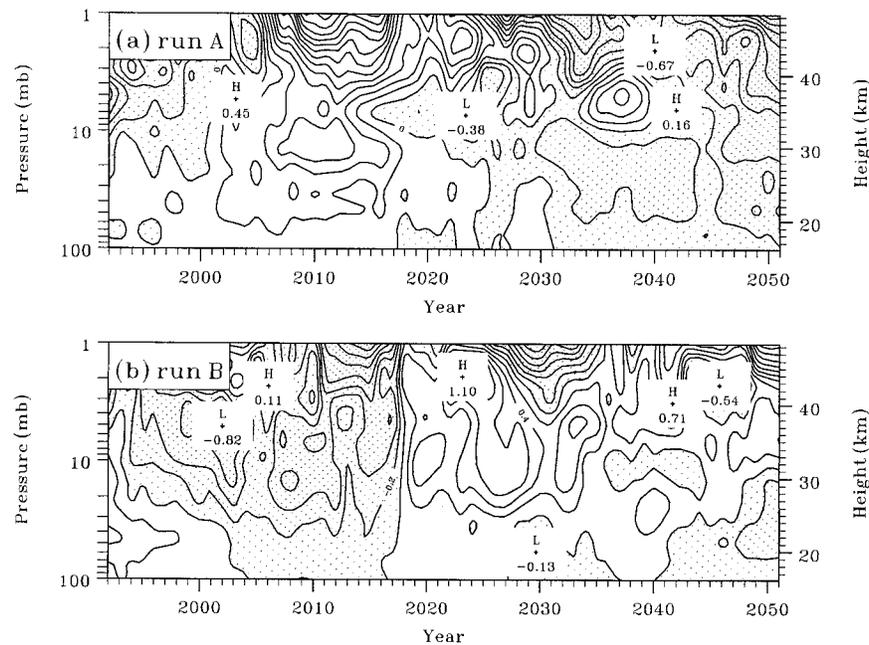Interestingly, the low-frequency variability in the

FIG. 6. Anomalous EP flux divergence expressed as a force per unit mass and averaged for DJF, and between 60° and 80°N for (a) run A and (b) run B. The anomalies are relative to the 60-yr mean for each integration and have been smoothed by an 11-yr running mean. Shading denotes convergence, which would act to weaken (strengthen) zonal mean westerly (easterly) winds [e.g., see right-hand term of Eq. (3.5.2a) of Andrews et al. (1987)] The contour interval is 0.2 m s⁻¹ day⁻¹.

lower and middle stratosphere in Fig. 5 does not appear in the area-averaged DJF temperatures for the troposphere, where both simulations produced almost the same systematic warming (cf. Figs. 5a and 5b), consistent with other models (e.g., Houghton et al. 1996). Similarly in the upper stratosphere there is a clear cooling signal in both simulations though there are quantitive differences (Fig. 5, see also Fig. 3b), possibly as a result of the variability of the response in the lower-to-middle stratosphere. In general, for the DJF zonal mean temperatures, the low-frequency variability was almost entirely confined to the north polar region and no compensatory response could be identified for the mean temperatures in other latitude bands.

### b. Stratospheric response to tropospheric forcing

The absence of a signal in the area-averaged temperatures for the troposphere does not exclude a change in the tropospheric forcing of the low-frequency internal atmospheric variability aloft. Figure 7 (solid curves) shows for both simulations the variations over the 60 yr in the mean upward DJF EP flux [$F_z$—Andrews et al. 1987, Eq. (3.5.3b)] at 100 mb for the region poleward of 40°N. The fluxes shown are anomalies from the 60-yr mean, smoothed by taking an 11-yr running mean, and further detrended by removing a least-squares fit linear trend—the straight lines in the figure. For comparison the area averaged DJF temperature anomalies

poleward of 60°N at 10 mb are also shown by the dashed curves in the picture. Again an 11-yr smoothing has been applied to the results and the linear trend separated out.

All the trends shown in Fig. 7, apart from the temperature trend in Fig. 7a, are statistically significant at the 95% confidence level, assuming the DJF means are statistically independent. Both simulations predicted a long-term increase in the upward flux of wave activity from the troposphere. The stronger trend in $F_z$ at 100 mb in run A is consistent with a greater increase in the adiabatic heating of the polar stratosphere, which, in turn, offsets the radiative cooling due to the increasing GHG concentrations more in run A than in run B. Hence the smaller downward trend in temperature in Fig. 7a (see also Fig. 3b).

The decadal variability in the 10-mb high-latitude DJF temperatures (dashed curves in Fig. 7) correlated reasonably well with the decadal variability in $F_z$ at 100 mb (solid curves) in both integrations (coefficients 0.87 and 0.48 for runs A and B, respectively). Again the correlations were consistent with basic dynamical theory, with anomalously warm (cold) winters nearly always occurring when there was an anomalously high (low) flux of wave activity from the troposphere. However, it is still unclear how much of the flux variability resulted directly from variability in the tropospheric source and how much was due to a modulation of the wave propagation by the stratosphere. Moreover, in run
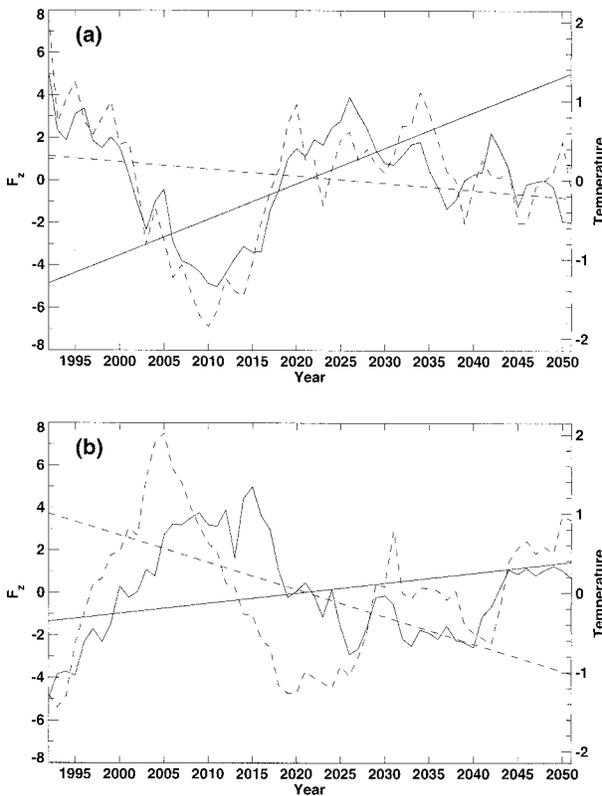
FIG. 7. For (a) run A and (b) run B. Solid curves: vertical component of the EP flux ($F_z$) at 100 mb averaged from 40°N to the pole ($10^{-3}$ Kg s$^{-2}$). Dashed curves: mean temperature poleward of 60°N at 10 mb (K). The results shown are means for DJF and are presented as anomalies from the 60-yr mean, smoothed with an 11-yr running mean and separated into a best-fit linear trend (straight lines) and the residual variability.

B, a higher correlation (0.65) was obtained when the midlatitude flux (20°–70°N) was considered instead of that poleward of 40°N, whereas in run A, the highest correlations came from the high latitudes.

About two-thirds of the total DJF EP flux through the 100-mb surface in the model came from the contribution from the monthly mean stationary waves (i.e., $F_z$ calculated from the monthly mean fields instead of the daily fields). This quasi-stationary wave component accounted almost entirely for the different trends shown in Fig. 7, and also for most of the correlation with the DJF 10-mb temperatures (results not shown). Thus differences in the stationary wave forcing from the troposphere appear to be the most likely cause of the uncertainties or, at least, the differences in the predicted stratospheric temperatures for the northern winter in the two integrations. On the other hand, both integrations predicted almost identical increases over the 60 yr in the transient component of $F_z$ through the 100-mb surface, or more precisely the residual on subtracting the contribution of the monthly mean stationary waves from the full $F_z$. The trends were statistically significant and, presumably, resulted from changes in midlatitude variability in

the troposphere similar to those found by Carnell and Senior (1998) with increasing GHG concentrations in a coupled ocean–atmosphere experiment using a version of the UM without our extended vertical domain.

### c. Sudden stratospheric warmings

As has been noted from other studies (e.g., Mahfouf et al. 1994; Rind et al. 1998) the responses shown in Figs. 5 and 6 were not just a manifestation of a uniform change throughout each winter, but were also associated with a change in the frequency of occurrences of sudden stratospheric warmings within the model (cf. Figs. 5 and 8). Although Mahfouf et al. (1994) and Rind et al. (1998) obtained opposite results—Mahfouf et al. reported an enhancement in the occurrences of sudden warmings on doubling $CO_2$ whereas Rind et al. claimed a reduction—they both concluded that the change in the frequency of warmings resulted from the prescribed changes in external forcing (i.e., GHG concentrations and sea surface boundary conditions). However, the different behavior of the two simulations presented here suggests that it is due to internal atmospheric variability, at least for our particular model and experimental setup. Internal variability could also explain the discrepancy in the findings of Mahfouf et al. and Rind et al. It is difficult to establish whether such low-frequency internal variability will be a feature of the future stratosphere. In the absence of climate change other stratospheric GCMs have produced an unrealistic clustering of sudden warmings in neighboring years so that, although the overall frequency of major warmings is similar to that observed, a decade with warmings almost every year can be followed by a decade with very few warmings (e.g., Hamilton 1995; Erlebach et al. 1996). Our own 20-yr reference simulation had no *major* warmings in the first decade and three in the second. This is in contrast to the observed distribution of major warmings every 2 yr, or so, at least prior to 1992 (Labitzke and van Loon 1992), but the agreement may be improved by the advent of a tropical quasi-biennial oscillation (QBO) in numerical models (A. A. Scaife et al. 2000, manuscript submitted to *Geophys. Res. Lett.*). For instance, Hamilton (1998) found that imposing a QBO in the modeled tropical winds eliminated the clustering of warmings and consequently increased the biennial component of the variability in the extratropics. This suggests that the QBO may remove some of the low-frequency variability in the occurrence of sudden warmings and thereby reduce some of the current uncertainty in the climate predictions for the polar stratosphere.

Of course, it is also possible that increased irregularity in the occurrences of major stratospheric warmings may be a real feature of climate change. For instance, between 1951 and 1992 the largest period between two major warmings was 4 yr. Then after 1992, until 1998, there were no major warmings, though the QBO was nearly always in its westerly phase during those six
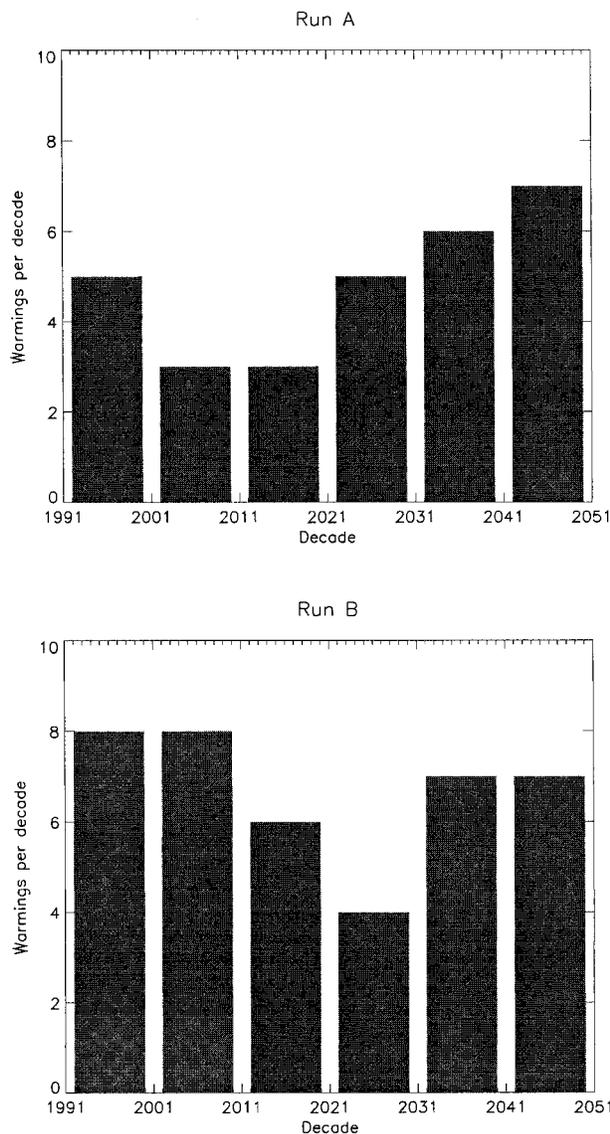
## Run A



## Run B

FIG. 8. Number of major sudden stratospheric warmings [i.e., reversal of the zonal mean westerly wind at 60°N and 10 mb (Andrews et al. 1987)] per decade occurring in DJF for (a: top) run A and (b: bottom) run B.

winters, which may partially account for the absence of warmings. So once again it appears that a realistic representation of the QBO in GCMs may be a prerequisite for accurately simulating present and future distributions of sudden warmings.

## 6. Southern Hemisphere winter and spring

### a. Trends and low-frequency variability

In the Southern Hemisphere the polar vortex is much more stable than its Northern Hemisphere counterpart. Nonetheless there was still sufficient interannual variability in the model results to mask any obvious trends

in the mean temperatures south of 60°S averaged over June–August (JJA). With an 11-yr smoothing, however, a cooling of the stratosphere can be identified in the results of both simulations presented in Fig. 9. Again, as in the northern winter, superimposed on the cooling trend were decadal variations, mainly of dynamical origins.

### b. Stratospheric response to tropospheric forcing

In both simulations, the temperature variations at 10 mb were well correlated (coefficients 0.86 and 0.88 for runs A and B, respectively) with the variations in the mean upward EP flux south of 40°S at 100 mb averaged over JJA (see Fig. 10). As might be expected, the amplitude of these decadal variations in EP fluxes and temperatures were much less than in the northern winter (cf. Figs. 7 and 10), representing a significant improvement from the earlier build of the troposphere–stratosphere configuration of the UM used by Butchart and Austin (1998). In their analyses of the model's climatology it was found that the southern winter was dynamically overactive and prone to producing the occasional spurious sudden warming (Butchart and Austin 1998).

At 100 mb, the average flux of wave activity, $F_z$, entering the Southern Hemisphere stratosphere during winter was between 60% and 65% of the flux diagnosed for the Northern Hemisphere winter. This was due to a smaller contribution from the monthly mean stationary waves that accounted for about 28% of the total flux as opposed to 69% in the Northern Hemisphere. Nonetheless, as for the northern winter, most of the correlation between $F_z$ and the 10-mb temperatures seen in Fig. 10 actually came from the stationary wave component (results not shown).

Again, as in the northern winter, the different trends in the JJA mean $F_z$ at 100 mb from runs A and B (cf. Figs. 10a and 10b) resulted almost entirely from differences in the contribution from the monthly mean stationary waves. On the other hand, for each simulation, the positive trend in the upward component of the full EP flux shown in Fig. 10 were statistically significant (assuming each year was independent), but the effects of the increased wave forcing were more than offset by the greenhouse cooling resulting in a stronger more stable polar vortex.

### c. Transition from winter to summer conditions

Yamaguchi and Hirooka (1996) examined 13 yr of observed winds and temperatures at 10 mb from 1980 to 1992 for trends in the date of the final Southern Hemisphere warming, but found no conclusive evidence for a shift. This is, perhaps, not surprising given the large interannual variability in the timing of the spring breakdown shown in Fig. 11 for our simulations. With the 60 yr of model data a statistically significant trend
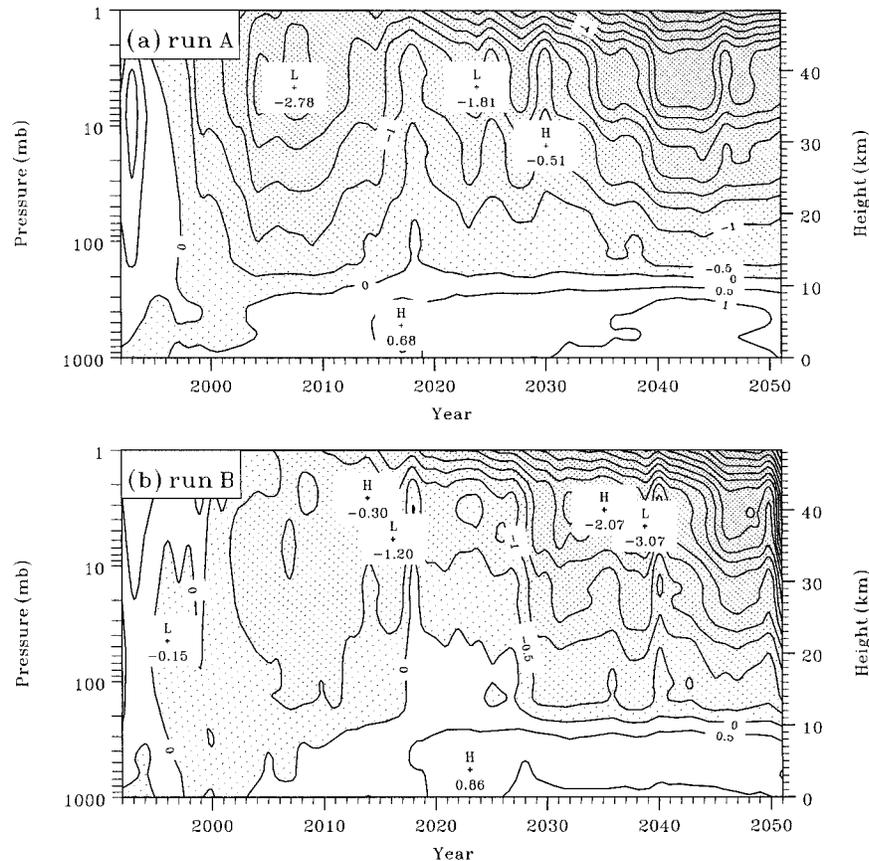
FIG. 9. As Fig. 5 but for the region poleward of 60°S and for JJA.

can, however, be isolated from the variability. Indeed, by spring there was enhanced cooling in the south polar region (see Fig. 4) in both simulations, though especially run A. Consequently the polar vortex lasted longer, on average, breaking down approximately 1–2 days later after each decade (see Fig. 11). Such a trend could, eventually, have important repercussions for the duration of the ozone hole. In particular, if an ozone hole were still to form by the middle of the next century the results here suggest that the low ozone levels could persist later in the year when they would lead to increases in UV penetration. Furthermore, this study took no account of the effects of the reduced ozone levels themselves, which are generally thought (e.g., Mahlman et al. 1994) to extend the duration of the polar vortex.

## 7. Polar stratospheric clouds

The potential for a long-term cooling of the high-latitude lower-stratosphere has important implications for future ozone depletion in that region due to the possibility of increased amounts of PSCs. These allow surface reactions, which lead to rapid local ozone losses in the polar spring in both hemispheres (Crutzen and Arnold 1986; Salawitch et al. 1990). The occurrence of

these clouds relies on low temperature thresholds being met, suggesting that, unlike other stratospheric aerosols, large increases may result from a reduction in temperature. Although theories of PSC formation are far from complete, it is well established that nitric acid containing particles are present at temperatures below about 195 K in the lower stratosphere (''type I'' PSCs), with water ice clouds (''type II'' PSCs) occurring 5–10 K below this (Turco et al. 1989). Type I PSCs are often identified with nitric acid trihydrate (NAT) due to its thermodynamic stability under similar physical conditions (Hanson and Mauersberger 1988), and this composition is often assumed in three-dimensional stratospheric chemistry model studies (e.g., Lefèvre et al. 1994; Chipperfield et al. 1996), although ternary solution droplets frequently appear to be present in observed PSCs (Dye et al. 1992; Carslaw et al. 1994). Here we have assessed possible changes in future PSC amounts using the thermodynamic NAT PSC representation used by Butchart and Austin (1996). This gave a better indication of the effect of climate change on chemistry than temperature alone. Indeed, a conventional analysis of seasonal minimum temperatures predicted in the simulations (not discussed here) showed markedly less significant trend information. Moreover, because of the similarity between
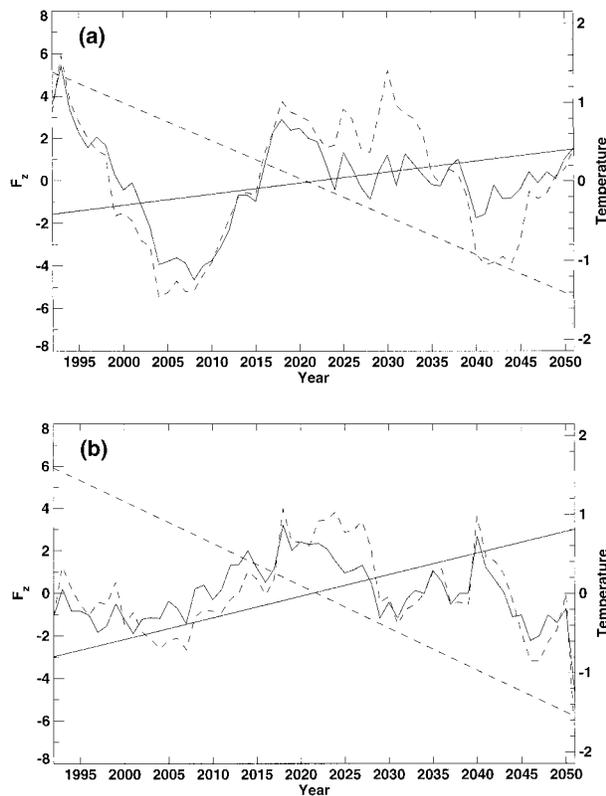
FIG. 10. As Fig. 7 but for the JJA EP flux poleward of 40°S and JJA 10-mb temperatures poleward of 60°S.

the temperature dependences of liquid and NAT PSC types the NAT scheme is adequate for assessing future PSC amounts, regardless of the exact nature of the particles.

### a. Northern Hemisphere

In the Arctic, winter minimum temperatures are often close to the threshold for type I PSC formation, causing PSCs to be sporadic and highly dependent on the meteorological details of the particular winter (Pawson et al. 1995). As has already been seen in section 5, interannual variability in the north significantly hampers attempts to detect systematic temperature trends. This also causes a high degree of variability in PSC amounts. The present marginal nature of Arctic PSCs implies that if winter temperatures decrease in the future, even by a small amount, significant increases in the frequency and intensity of PSCs and thus ozone depletion could occur. Under current conditions temperatures are rarely low enough for type II PSC formation, and are not predicted to become so, during the period considered here.

We derive, from our predicted temperatures changes, Northern Hemisphere PSC trends in terms of the surface area density (SAD), which represents the amount of surface area available for chemical reactions on PSC particles per unit volume. Although the ozone response
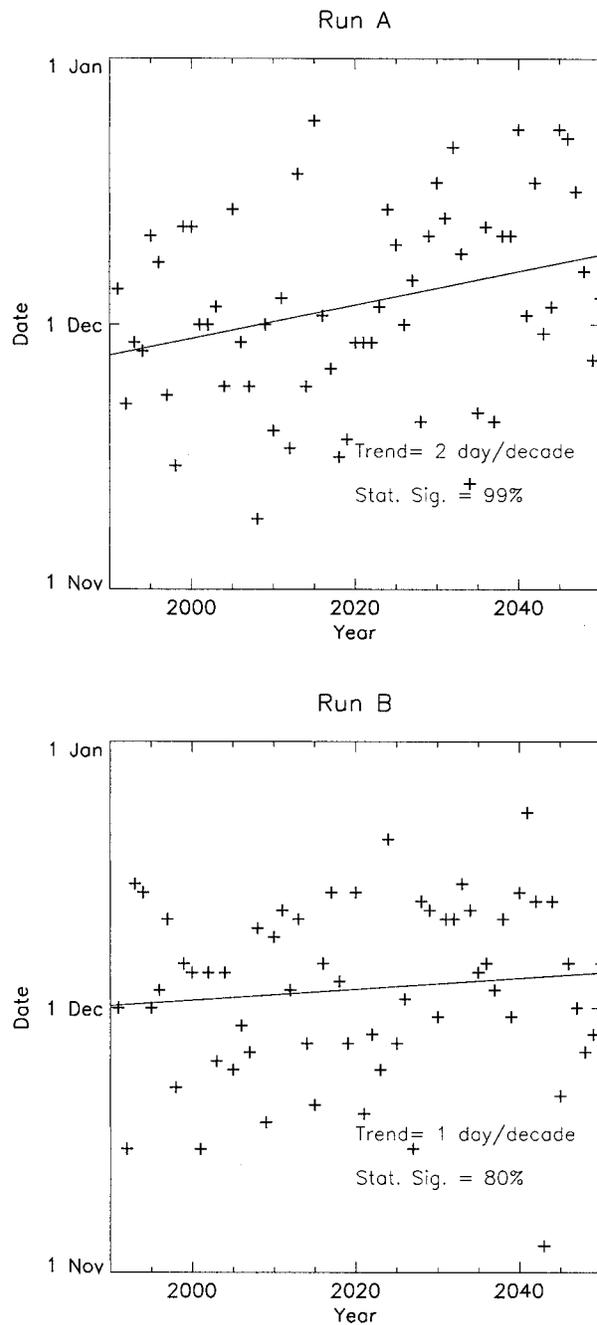


FIG. 11. Date of the transition to summer easterlies at 10 mb and 60°S in (a: top) run A and (b: bottom) run B. The least squares fit to the data is also indicated.

is nonlinear and relies on a number of other factors, this quantity has more relevance to PSC chemistry than temperature and is perhaps the best indicator of possible future trends in Arctic ozone depletion in GCM simulations without chemistry. Assuming fixed concentrations of nitric acid and water vapor typical of the polar lower stratosphere (here 10 ppb by volume and 4.5 ppm by volume, respectively), the amount of nitric acid con-
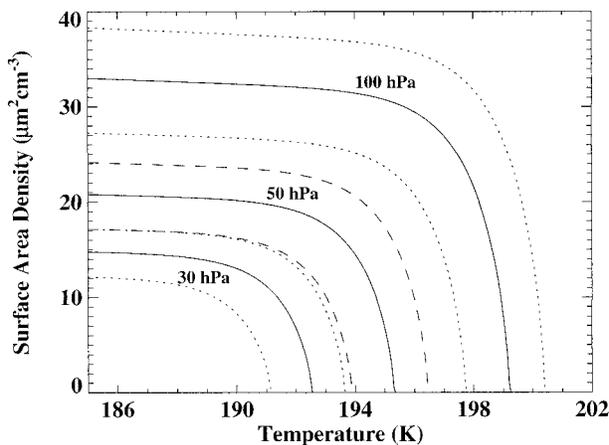
FIG. 12. SAD ($\mu$m$^2$ cm$^{-3}$) as a function of temperature at 100, 50, and 30 mb assuming ambient concentrations of nitric acid and water vapor of 4.5 ppmv and 10 ppbv, respectively (solid lines), using the thermodynamic equilibrium representation of Hanson and Mauersberger (1988). Upper and lower uncertainty estimates are shown as dotted (100 and 30 mb) and dashed (50 mb) lines, using nitric acid and water vapor values of 3.5 ppmv and 7.5 ppbv for the lower limit and 5.5 ppmv and 12.5 ppbv for the upper limit.

tained within NAT particles (as opposed to the gas phase) was calculated using the PSC scheme from the model of Butchart and Austin (1996). From this, the density of NAT (Drdla and Turco 1991), and the assumption of locally identical spherical particles of number density 10 cm$^{-3}$, the surface area density was calculated. The dependence of SAD on temperature is shown in Fig. 12 for 100, 50, and 30 mb, both for the assumed water vapor and nitric acid concentrations and for other cases (see figure legend for details), thus indicating the sensitivity. Larger surface areas are produced lower down, with condensation of NAT particles quickly rising from zero to a limiting value set by the availability of nitric acid. At each level this limit is 16% higher and 18% lower for the cases with the different concentrations of nitric acid and water vapor, showing that the calculated surface area density is sufficiently insensitive to these uncertainties to be a useful measure of likely PSC amounts.

Figure 13 shows the change in PSCs for each winter (taken as November–March) in the two calculations, A and B, at 31 mb. In (a), the SAD integrated over the region where PSCs would occur is shown for each day of every winter season in the runs. PSCs often appeared in late November or early December, however, in some years PSC threshold temperatures were not reached until into January. Although some PSCs would occur in every model year, in certain years they lasted for only a few days (e.g., 1995/6 and 2031/2 in run A, and 2007/8 and 2024/5 in run B). The date of the last PSCs varied widely between January and March, although the strongest intensities, corresponding to the most widespread clouds, were clustered in late December, January and early February. The differences between the integrations are most

apparent in the dynamically active late winter and early spring, reflecting the differing decadal-length variation in the frequency of sudden stratospheric warmings. For example, the lack of warmings in the decade 2005–15 in run A (corresponding to the low-temperature period in Fig. 5) is associated with PSCs predicted to last into March for nine consecutive years. Similarly, the decade 2000–10 in run B has a higher than average number of warmings (Fig. 8) with a comparative paucity of PSCs.

Integrating these daily SAD amounts across the winter gives a measure of the total PSC activity in each winter, plotted as a function of time in Fig. 13b for 31 mb. The best-fit linear trend is also shown, indicating that overall PSCs increase by 60% and 100% from 1992 to 2051 in runs A and B, respectively. Using a two-tailed $t$ test on these results gives confidence intervals of 87% (run A) and 98% (run B), showing that the predicted PSC enhancement is likely to be a robust result of the systematic stratospheric changes rather than an artifact of the large variability. At lower altitudes, however, the PSC trends (not shown) are smaller because of the weaker cooling, and are less statistically significant. As a function of date and latitude the 31-mb PSC trends are shown in Fig. 14. The largest and most significant trends occur in December in both calculations, and although some significant increases occur in late January in run B, they are not corroborated by run A. This pattern reflects the contrast between the more reliable cooling trend in the radiatively controlled early winter and the uncertain trend due to decadal variability in the sudden warming frequency later in the season (Fig. 4). Pawson et al. (1995) also see such a difference between early and late winter in analysis temperatures for 1965/6 through 1993/4. In their study it was found that the extent of temperatures below 192 K at 30 mb in December and January was greater on average during the last 18 yr, but was not significantly different during February. Lack of sunlight means that the predicted increase in PSCs in December does not have the same direct implications for additional ozone depletion that it would have in late winter or early spring. It has been suggested, however, that long-lived PSCs may be associated with denitrification (Santee et al. 1998; Waibel et al. 1999) and, therefore, increases in early winter PSCs could increase ozone loss later on (Chipperfield and Pyle 1998).

### b. Southern Hemisphere

Antarctic winters are sufficiently cold and undisturbed to allow substantial type I PSCs and, to a lesser extent type II PSCs, to exist for a long continuous period in the lower stratosphere. As a result, chlorine and bromine are in active forms throughout the polar vortex for a large fraction of the winter and ozone depletion proceeds at the maximum rate. Decreases in temperature leading to increases in PSC amounts, therefore, would not have much impact on ozone loss under these con-
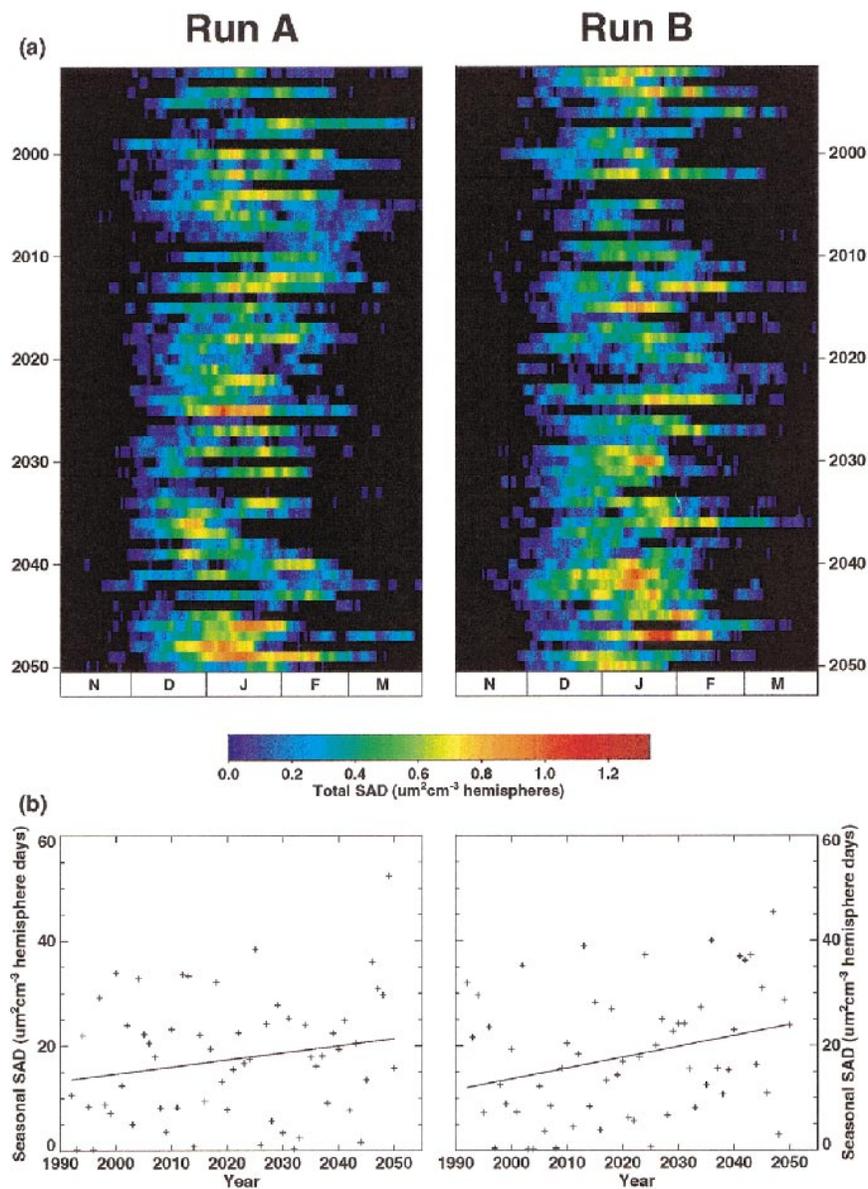
FIG. 13. (a) Arctic winter SAD expressed as an area integral amount ($\mu m^2$ cm$^{-3}$ hemispheres) for each day (Nov–Mar) of the modeled seasons 1991–92 to 2050–51 at 31 mb in runs A and B. (b) Total seasonal SAD derived by summing the results in (a) for each year ($\mu m^2$ cm$^{-3}$ hemisphere days; crosses). The best-fit linear trend for each run is also shown.

ditions. It is at the margins of PSC activity, at the vortex edge or at the top of the current PSC region or at the beginning and end of the winter that additional PSCs could affect ozone amounts. Hence for the southern winter we examine the extent of the area where PSCs occur rather than the surface area density.

The May–November mean trends in the zonally averaged occurrences of type I PSCs (% decade$^{-1}$) are shown in Fig. 15. In both calculations the largest and most significant changes occurred between 60°S and 70°S and in the polar region above 15 mb. This reflects

the tendency for the predicted climate change to extend both upward and equatorward the region where PSCs are prevalent for a large part of the winter. The trends in occurrence of type I PSCs increase with height in response to the larger cooling higher up (Fig. 9) and are in reasonable agreement where significance is found in both simulations. Changes in type II PSC formation are not included in Fig. 15. In practice, the region affected by ice clouds lies south of 70°S, where the runs do not show agreed significance and where chlorine and bromine activation would be expected to be complete.
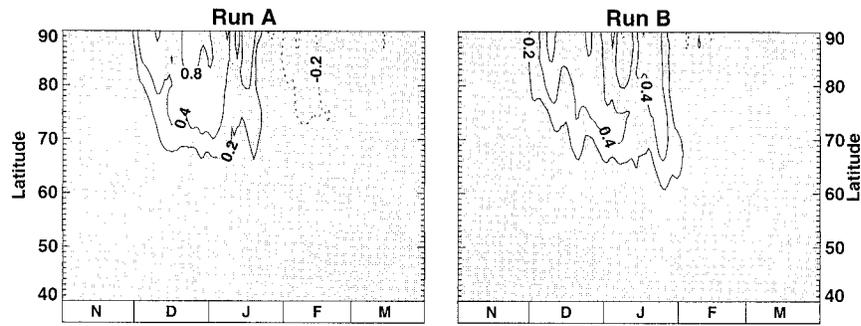
FIG. 14. Zonal mean SAD decadal trends ($\mu$m$^2$ cm$^{-3}$) at 31 mb in winter and spring as a function of time and latitude. The trend data have been smoothed in time by applying a 5-day running mean. Contours for positive values are solid and contours for negative values are dashed. Shading denotes trends that are not statistically significant at the 95% confidence interval using the same $t$ test as in Fig. 3. The significance information has no time smoothing.

It is worth noting, however, that increases in ice amounts could lead to additional ozone depletion by increasing denitrification.

Figure 16 shows the intraseasonal distribution of these changes at 31 mb. Both calculations imply increases in type I PSCs during the formation of the vortex and in October, and also at the vortex edge. The largest changes are predicted to occur by the progressively earlier onset of PSCs, similar to the early season trend in the Arctic. The statistical significance of the increases is more intermittent later in the spring, due to the growing influence of planetary wave perturbations. There are, however, periods in both runs even in September and October, which show significant positive trends in PSC occurrences. As this corresponds to the time when the Antarctic ozone hole forms, this implies the potential for the enhancement of ozone depletion.

## 8. Concluding remarks

The global mean stratosphere is fairly close to radiative equilibrium and therefore changes in the concentrations of the radiatively active trace gases have a more direct impact on the climate there than at the earth's surface. Nonetheless, unlike in the troposphere, each of the well-mixed GHGs behaves differently so that the combined radiative forcing cannot be properly represented by specifying an ''equivalent $CO_2$'' concentration (e.g., see World Meteorological Organization 1999, chapter 5), as is common in many climate prediction studies (e.g., Mitchell and Johns 1997). In the GCM used in this study the flexible new radiation code developed by Edwards and Slingo (1996) was included to calculate the longwave cooling using the IPCC's IS92a projected concentrations of each of $CH_4$, $N_2O$, CFC11, and CFC12, as well as $CO_2$ (Fig. 1). Two simulations (identical, apart from initial conditions) using this model produced the same secular global cooling of the stratosphere between 1992 and 2051 with the signal more clearly detectable than the corresponding global warming of the troposphere, which was modulated on a decadal timescale by the effects of the SSTs. In our model this global decadal variability did not extend significantly above the tropopause confirming that the stratosphere will probably be the best region for early detection of the effects of anthropogenic emissions on the global climate.
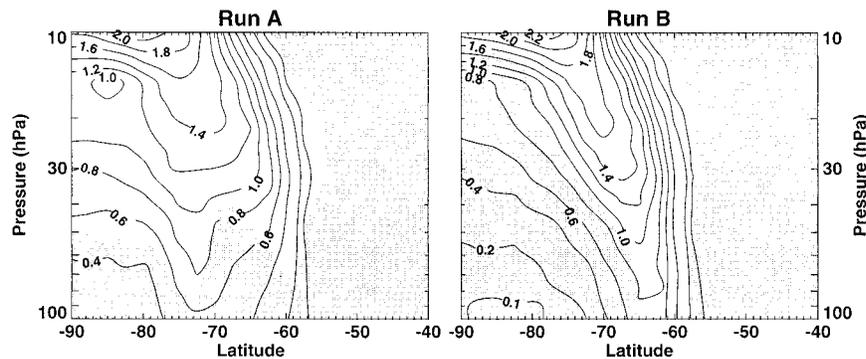
Critically, despite the unambiguous prediction of a



FIG. 15. Trend in the zonal mean occurrences of type I PSCs averaged over the Antarctic winter (taken as May–Oct inclusive; % decade$^{-1}$). The shading has the same interpretation as in Fig. 14.
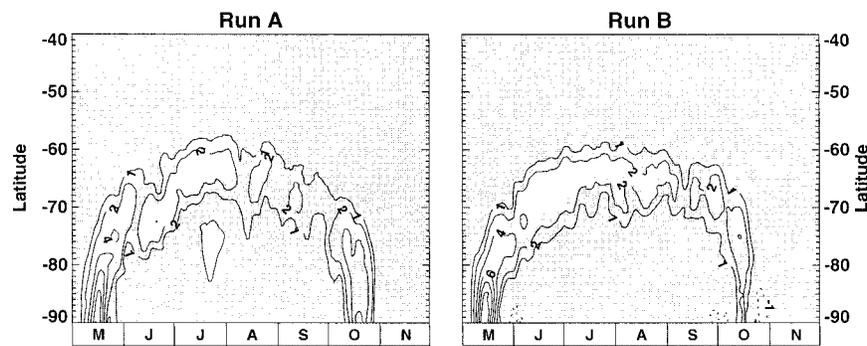
FIG. 16. Trend in the zonal mean occurrences of type I PSCs in Antarctic winter and spring as a function of time and latitude, (% decade$^{-1}$). Contours for positive values are solid and contours for negative values are dashed. The shading has the same interpretation as in Fig. 14. The trends have been smoothed in time by applying a 5-day running mean, whereas the significance information has no time smoothing.

global cooling of the stratosphere, we also found that reliable quantitative predictions of the temperature trend in the polar low and middle stratosphere were not possible from a single integration of our particular model. Indeed, during the winter months the model temperatures in the polar stratosphere varied on a decadal time-scale by a comparable amount to the secular changes over the same period. Because results were available from two simulations we were able to establish firmly that this low-frequency variability was internal, and not the result of the changes in external forcing (e.g., SSTs and GHG concentrations). In both hemispheres it originated predominately from the variability in the flux of quasi-stationary wave activity from the troposphere though it was not possible to distinguish whether this was due to a modulation of the wave propagation by the stratosphere or changes in the tropospheric sources of the waves. If a modulation were responsible then, as discussed in section 5, improving the model to enable it to reproduce a realistic equatorial QBO may reduce the amplitude of the decadal variability and allow useful predictions of trends to be made from a single integration. On the other hand, the variability could correspond to a natural mode of the real atmosphere, such as that which associates a strengthened polar night vortex with an enhanced North Atlantic oscillation (e.g., Graf et al. 1995, 1998). Ensembles of integrations may then be required to extract useful information. Furthermore, evidence for natural modes of variability coupling the troposphere and stratosphere suggest a possible weakness in our approach of deriving SSTs from a model with a limited representation of the stratosphere (Shindell et al. 1999), which could be addressed only when OAGCMs become available with extended vertical domains.

Although most of the uncertainties in our predictions were associated with the stationary waves we also found that there was a statistically significant increase in the upward flux of transient wave activity at the tropopause. This was consistent with the predicted changes in daily

variability in the climate version of the UM (Carnell and Senior 1998) and produced an increase in the dynamical heating of the polar regions during winter. However, this was small by comparison with the additional radiative cooling that came from the increasing total GHG forcing, especially in the Southern Hemisphere where the net effect was that the polar vortex became more stable over the 60 yr, with its duration extended by 1–2 days per decade.

In our simulations the monthly mean stationary waves provided just over two-thirds of the Northern Hemisphere flux of wave activity from the troposphere. The decadal variability in this flux induced a similar variability in the stratospheric temperatures in high latitudes though this was not uniform throughout the winter. Instead the frequency of occurrences of major stratospheric warmings per decade varied in a nonsecular manner and differently in our two simulations. As this was an internal mode of variability that did not appear to be forced by the increasing GHG concentrations, it suggests that predictions of the decadal mean Arctic ozone depletion that depend on a change in the likelihood of sudden stratospheric warmings (Shindell et al. 1998; World Meteorological Organization 1999, chapter 12) may not be altogether reliable. On the other hand, the calculations of Shindell et al. (1998) took account of the changing ozone levels in the radiative forcing and that could, possibly, reduce the uncertainties resulting from the low-frequency variability in the dynamics.

One of the most important impacts of climate change will be the effects on stratospheric ozone abundance and the amount of UV radiation reaching the ground. The effects of climate change on PSC formation, in particular, is crucial to predicting the future severity of the seasonal polar ozone losses in late winter and early spring. Using a thermodynamic PSC representation similar to that used in three-dimensional chemical models we assessed the response of PSC amounts to our predicted temperature changes. In the Arctic the variability in the frequency of sudden warmings per decade was

found to be evident in the degree of persistence of PSC events into late winter. Nonetheless, the seasonal average, area-integrated PSC SAD was calculated to increase significantly by 60%–100% over the 60 yr at and above 31 mb, but the increases occurred mainly in the early winter. In the late winter, when additional ozone depletion is much more likely to result, the large variability resulted in trend predictions that were not significant. In the Antarctic, increases in the early part of the winter also occurred though, perhaps more importantly, the region of PSC formation was shown to extend both upward and equatorward in response to the stratospheric cooling. This is likely to have a similar effect on the future size of the ozone hole even if the local severity of the ozone loss were to decrease in response to the fall in inorganic chlorine amounts.

To date it has not been possible to integrate continuously for 60 yr a version of our model incorporating a full representation of the chemistry and transport of the species that determine the ozone distribution. Nonetheless such a comprehensive chemical-dynamical-transport model has been developed based on the UM and has been run for periods exceeding 16 months using initial meteorological conditions from the runs described here [see Austin et al. (2000) for details]. These relatively short integrations were then used to provide ''snapshots'' of how stratospheric ozone would behave at 5–15-yr intervals over the period 1979–2015 (Austin et al. 2000). However, it remains to be seen if the additional radiative feedbacks of the simulated ozone in a multiannual integration will dampen the internal decadal variability of the model and/or strengthen any trends in ozone amounts to make the predictions from a single integration more reliable. In addition, although our two integrations suggest that the decadal variability in the sea surface conditions may not affect the stratospheric global and annual mean trends, this is unlikely to be the case in the high latitudes in winter. A number of studies (e.g., van Loon and Labitzke 1987; Hamilton 1993a,b) have suggested a possible link between the stratospheric circulation anomalies and SSTs. Therefore, a reliable assessment of the future state of the stratospheric ozone layer will almost certainly have to be based on consensus between many modeling groups running their own fully coupled stratospheric chemistry-climate models to simulate conditions for the first half of the next century. This will be a major challenge for the relatively small number of stratospheric researchers but an essential task given the now recognized importance (Santer et al. 1996) of stratospheric ozone changes to surface climate.

### REFERENCES

Andrews, D. G., J. R. Holton, and C. B. Leovy, 1987: *Middle Atmosphere Dynamics.* Academic Press, 489 pp.

Austin, J., and N. Butchart, 1994: The influence of climate change and the timing of stratospheric warmings on Arctic ozone depletion. *J. Geophys. Res.,* **99,** 1127–1145.

——, ——, and K. Shine, 1992: Possibility of an Arctic ozone hole in a doubled-$CO_2$ climate. *Nature,* **360,** 221–225.

——, J. R. Knight, and N. Butchart, 2000: Three-dimensional chemical model simulations of the ozone layer: 1979–2015. *Quart. J. Roy. Meteor. Soc.,* in press.

Butchart, N., and J. Austin, 1996: On the relationship between the quasi-biennial oscillation, total chlorine and the severity of the antarctic ozone hole. *Quart. J. Roy. Meteor. Soc.,* **122,** 183–217.

——, and ——, 1998: Middle atmosphere climatologies from the troposphere–stratosphere configuration of the UKMO's unified model. *J. Atmos. Sci.,* **55,** 2782–2809.

Carnell, R. E., and C. A. Senior, 1998: Changes in mid-latitude variability due to increasing greenhouse gases and sulphate aerosols. *Climate Dyn.,* **14,** 369–383.

Carslaw, K. S., B. P. Luo, S. L. Clegg, Th. Peter, P. Brimblecombe, and P. J. Crutzen, 1994: Stratospheric aerosol growth and $HNO_3$ gas phase depletion from coupled $HNO_3$ and water uptake by liquid particles. *Geophys. Res. Lett.,* **21,** 2479–2482.

Chipperfield, M. P., and J. A. Pyle, 1996: Model sensitivity studies of ozone depletion. *J. Geophys. Res.,* **103,** 28 389–28 403.

——, A. M. Lee, and J. A. Pyle, 1996: Model calculations of ozone depletion in the Arctic polar vortex for 1991–1992 to 1994–1995. *Geophys. Res. Lett.,* **23,** 559–562.

Crutzen, P. J., and F. Arnold, 1986: Nitric acid cloud formation in the cold Antarctic stratosphere: A major cause of the springtime ''ozone hole.'' *Nature,* **324,** 651–655.

Cullen, M. J. P., 1993: The unified forecast/climate model. *Meteor. Mag.,* **122,** 81–94.

——, and T. Davies, 1991: A conservative split-explicit integration scheme with fourth-order horizontal advection. *Quart. J. Roy. Meteor. Soc.,* **117,** 993–1002.

Drdla, K., and R. P. Turco, 1991: Denitrification through PSC formation: A 1D model incorporating temperature oscillations. *J. Atmos. Chem.,* **12,** 319–366.

Dye, J. E., and Coauthors, 1992: Particle size distributions in Arctic polar stratospheric clouds. *J. Geophys. Res.,* **97,** 8015–8034.

Edwards, J. M., and A. Slingo, 1996: Studies with a flexible new radiation code. Part I: Choosing a configuration for a large-scale model. *Quart. J. Roy. Meteor. Soc.,* **122,** 689–719.

Erlebach, P., U. Langematz, and S. Pawson, 1996: Simulations of stratospheric sudden warmings in the Berlin troposphere–stratosphere–mesosphere GCM. *Ann. Geophys.,* **14,** 443–463.

Graf, H.-F., I. Kirchner, and J. Perlwitz, 1998: Changing lower stratospheric circulation: The role of ozone and greenhouse gases. *J. Geophys. Res.,* **103,** 11 251–11 261.

——, J. Perlwitz, I. Kirchner, and I. Schult, 1995: Recent northern winter climate trends, ozone changes and increased greenhouse gas forcing. *Contrib. Phys. Atmos.,* **68,** 233–248.

Gregory, D., G. J. Shutts, and J. R. Mitchell, 1998: A new gravity-wave-drag scheme incorporating anisotropic orography and low-level wave breaking: Impact upon the climate of the UK Meteorological Office unified model. *Quart. J. Roy. Meteor. Soc.,* **124,** 463–493.

Hamilton, K., 1993a: An examination of observed Southern Oscillation effects in the northern stratosphere. *J. Atmos. Sci.,* **50,** 44–66.

——, 1993b: A general circulation model simulation of El Niño effects in the extratropical northern stratosphere. *Geophys. Res. Lett.,* **20,** 1803–1806.

——, 1995: Interannual variability in the Northern Hemisphere winter middle atmosphere in control and perturbed experiments with the GFDL SKYHI general circulation model. *J. Atmos. Sci.,* **52,** 44–66.

——, 1996: Comprehensive meteorological modelling of the middle atmosphere: A tutorial review. *J. Atmos. Terr. Phys.,* **58,** 1591–1627.

——, 1998: Effects of an imposed quasi-biennial oscillation in a comprehensive troposphere–stratosphere–mesosphere general circulation model. *J. Atmos. Sci.,* **55,** 2393–2418.

Hansen, J. E., M. Sato, R. Ruedy, A. Lacis, and J. Glascoe, 1998: Global climate data and models: A reconciliation. *Science,* **281,** 230–232.

Hanson, D., and K. Mauersberger, 1988: Laboratory studies of the nitric acid trihydrate: Implications for the south polar stratosphere. *Geophys. Res. Lett.,* **15,** 855–858.

Houghton, J. T., L. G. Meira Filho, B. A. Callander, N. Harris, A. Kattenberg, and K. Maskell, Eds., 1996: *Climate Change 1995.* Cambridge University Press, 572 pp.

Johns, T. C., R. E. Carnell, J. F. Crossley, J. M. Gregory, J. F. B. Mitchell, C. A. Senior, S. F. B. Tett, and R. A. Wood, 1997: The second Hadley Centre coupled ocean–atmosphere GCM: Model description, spinup and validation. *Climate Dyn.,* **13,** 103–134.

Keating, G. M., D. F. Young, and M. C. Pitts, 1987: Ozone reference models for CIRA. *Adv. Space Res.,* **7,** 105–115.

Labitzke, K., and H. van Loon, 1992: On the association between the QBO and the extratropical stratosphere. *J. Atmos. Terr. Phys.,* **54,** 1453–1463.

Lefèvre, F., G. P. Brasseur, I. Folkins, A. K. Smith, and P. Simon, 1994: Chemistry of the 1991–1992 stratospheric winter: Three-dimensional model simulations. *J. Geophys. Res.,* **99,** 8183–8195.

Mahfouf, J. F., D. Cariolle, J.-F. Geleyn, and B. Timbal, 1994: Response of the Météo-France climate model to changes in $CO_2$ and sea surface temperature. *Climate Dyn.,* **9,** 345–362.

Mahlman, J. D., J. P. Pinto, and L. J. Umscheid, 1994: Transport, radiative, and dynamical effects of the Antarctic ozone hole: A GFDL ''SKYHI'' model experiment. *J. Atmos. Sci.,* **51,** 489–508.

Mitchell, J. F. B., and T. C. Johns, 1997: On the modification of global warming by sulphate aerosols. *J. Climate,* **10,** 245–267.

——, ——, J. M. Gregory, and S. F. B. Tett, 1995: Climate response to increasing levels of greenhouse gases and sulphate aerosols. *Nature,* **376,** 501–504.

Palmer, T. N., G. J. Shutts, and R. Swinbank, 1986: Alleviation of a systematic westerly bias in general circulation and numerical weather prediction models through an orographic gravity wave drag parametrization. *Quart. J. Roy. Meteor. Soc.,* **112,** 1001–1039.

Pawson, S., and B. Naujokat, 1997: Trends in daily wintertime temperatures in the northern stratosphere. *Geophys. Res. Lett.,* **24,** 575–578.

——, ——, and K. Labitzke, 1995: On the polar stratospheric cloud formation potential of the stratosphere. *J. Geophys. Res.,* **100,** 23 215–23 225.

——, and Coauthors, 2000: The GCM–Reality Intercomparison Project for SPARC (GRIPS): Scientific issues and initial results. *Bull. Amer. Meteor. Soc.,* **81,** 781–796.

Pitari, G., S. Palermi, G. Visconti, and R. G. Prinn, 1992: Ozone response to a $CO_2$ doubling: Results from a stratospheric general circulation model with heterogeneous chemistry. *J. Geophys. Res.,* **97,** 5953–5962.

Pope, V. D., M. Gallani, P. R. Rowntree, and R. Stratton, 2000: The impact of new physical parametrizations in the Hadley Centre climate model—HadAM3. *Climate Dyn.,* **16,** 123–146.

Ramaswamy, V., M. D. Schwarzkopf, and W. J. Randel, 1996: Fingerprint of ozone depletion and temporal pattern of recent lower-stratospheric cooling. *Nature,* **382,** 616–618.

Rind, D., D. Shindell, P, Lonergan, and N. K. Balachandran, 1998: Climate change and the middle atmosphere. Part III: The doubled $CO_2$ climate revisited. *J. Climate,* **11,** 876–894.

Salawitch, R. J., and Coauthors, 1990: Loss of ozone in the Arctic vortex for the winter of 1989. *Geophys. Res. Lett.,* **17,** 561–564.

Santee, M. L., A. Tabazadeh, G. L. Manney, R. J. Salawitch, L. Froidevaux, W. G. Read, and J. W. Waters, 1998: UARS microwave limb sounder $HNO_3$ observations: Implications for Antarctic polar stratospheric clouds. *J. Geophys. Res.,* **103,** 13 258–13 313.

Santer, B. D., and Coauthors, 1996: A search for human influences on the thermal structure of the atmosphere. *Nature,* **382,** 39–46.

Shindell, D. T., D. Rind, and P. Lonergan, 1998: Increased polar stratospheric ozone losses and delayed eventual recovery owing to increasing greenhouse-gas concentrations. *Nature,* **392,** 589–592.

——, R. L. Miller, G. A. Schmidt, and L. Pandolfo, 1999: Simulation of recent northern winter climate trends by greenhouse-gas forcing. *Nature,* **399,** 452–455.

Scaife, A. A., J. Austin, N. Butchart, S. Pawson, M. Keil, J. Nash, and I. N. James, 2000: Seasonal and interannual variability of the stratosphere diagnosed from UKMO TOVS analyses. *Quart. J. Roy. Meteor. Soc.,* in press.

Swinbank, R., and A. O'Neill, 1994: A stratosphere–troposphere data assimilation system. *Mon. Wea. Rev.,* **122,** 686–702.

——, W. A. Lahoz, A. O'Neill, C. S. Douglas, A. Heaps, and D. Podd, 1998: Middle atmosphere variability in the Meteorological Office unified model. *Quart. J. Roy. Meteor. Soc.,* **124,** 1485–1526.

Timbal, B., J.-F. Mahfouf, J.-F. Royer, U. Cubasch, and J. M. Murphy, 1997: Comparison between doubled $CO_2$ time-slice and coupled experiments. *J. Climate,* **10,** 1463–1469.

Turco, R. P., O. B. Toon, and P. Hamil, 1989: Heterogeneous physicochemistry of the polar ozone hole. *J. Geophys. Res.,* **94,** 16 493–16 510.

van Loon, H., and K. Labitzke, 1987: The Southern Oscillation. Part V: The anomalies in the lower stratosphere of the Northern Hemisphere in winter and a comparison with the quasi-biennial oscillation. *Mon. Wea. Rev.,* **115,** 357–369.

Waibel, A. E., and Coauthors, 1999: Arctic ozone loss due to denitrification. *Science,* **283,** 2064–2069.

World Meteorological Organization, 1999: Scientific assessment of ozone depletion: 1998. Rep. No. 44, WMO Global Ozone Research and Monitoring Project, Geneva, Switzerland.

Yamaguchi, T., and T. Hirooka, 1996: Relationship between the depth of ozone hole and Southern Hemisphere stratospheric final warming (in Japanese). *J. Meteor. Soc. Japan,* **C110.**

Zurek, R. W., G. L. Manney, A. J. Miller, M. E. Gelman, and R. M. Nagatani, 1996: Interannual variability of the north pole vortex in the lower stratosphere during the UARS mission. *Geophys. Res. Lett.,* **23,** 289–292.